Experimental Investigation of the Mechanisms of Cellular Instabilities Developing on Spherical Two-Phase Flames

Romain Thimothée, Christian Chauveau, Fabien Halter, Iskender Gökalp

▶ **To cite this version:**

Romain Thimothée, Christian Chauveau, Fabien Halter, Iskender Gökalp. Experimental Investigation of the Mechanisms of Cellular Instabilities Developing on Spherical Two-Phase Flames. Combustion Science and Technology, 2016, 188 (11-12), pp.2026 - 2043. 10.1080/00102202.2016.1214421 . hal-01858476

HAL Id: hal-01858476

https://hal.science/hal-01858476v1

Submitted on 14 May 2024

HAL is a multi-disciplinary open access archive for the deposit and dissemination of scientific research documents, whether they are published or not. The documents may come from teaching and research institutions in France or abroad, or from public or private research centers.

L'archive ouverte pluridisciplinaire **HAL**, est destinée au dépôt et à la diffusion de documents scientifiques de niveau recherche, publiés ou non, émanant des établissements d'enseignement et de recherche français ou étrangers, des laboratoires publics ou privés.

Distributed under a Creative Commons Attribution - NonCommercial - NoDerivatives 4.0 International License

The publisher version is available using this link : https://doi.org/10.1080/00102202.2016.1214421

Experimental Investigation of the Mechanisms of Cellular Instabilities Developing on Spherical Two-phase Flames

R. Thimothée[1*], C. Chauveau[1], F. Halter[1] & I. Gökalp[1]

[1]*Institut de Combustion, Aérothermique, Réactivité et Environnement (ICARE), Centre National de la Recherche Scientifique, 1C avenue de la Recherche Scientifique, 45071 Orléans cedex 2, France*

Abstract

The presence of liquid fuel droplets in a flammable mixture causes cellular instabilities on the flame surface which significantly enhances the flame speed when compared to the fully vaporized case. The prediction of the mechanisms responsible for the onset of cellularity for two-phase mixtures is essential to better understand spray combustion. The present study considers an innovative experimental strategy to isolate and investigate any potential mechanisms. The fuel droplets were replaced by inert water droplets in order to amplify the thermal sink effect, characterized by the absorption of part the heat released by the flame, and to suppress the local enrichment of fuel formed around droplets. Spherical expanding flames with narrow-size distribution droplets were used and qualitative comparisons of the flame structure were performed with a shadowgraph system. The results have shown that the heat sink has no significant effect whereas the local enrichment of fuel appears as a key phenomenon which suggests that, in case of fuel droplet aerosols, the onset of cellularities is triggered in the inhomogeneous part of the gaseous phase.

Keywords: Aerosol combustion, water mist, spherical flame, cellular instabilities, thermal sink, water dilution

1. Introduction

Background

Spray combustion plays a major role in various domains such as motorization (spark ignition, diesel and turbojet engines) and in industrial applications (furnaces and boilers). It is well established that, under certain circumstances, the propagation speed of a flame through a fuel aerosol can be greatly higher than in the gaseous mixture with the same overall conditions (Ballal and Lefebvre, 1981, Myers and Lefebvre, 1986, Lin and Sheu, 1991, Nomura et al., 1998). Moreover, it was reported that two-phase flames propagate with a corrugated flame front and a cellular flame surface similar to those encountered with premixed gas mixtures. Hayashi et al. (1977) are the first to suggest the explanation, which is nowadays well-adopted, that the flame speed promotion was due to the peculiar cellular instabilities by increasing the flame surface area. Studies of Lawes et al. (2006) reported that aerosol flames become unstable earlier than gaseous flames, and with more pronounced instabilities characterized by a finer cellular structure. Additionally, experiments carried on with ethanol-air mixtures demonstrated that the presence of fuel droplets can produce cells development while the fully vaporized flame is totally stable and smooth, whether for lean and rich equivalence ratios (Thimothée et al., 2015).

A fast burning rate can be an advantage for engines but is a serious disadvantage in an industrial hazard context. The cellular aspect plays a main role in flame speed enhancement, thus the ability to predict the onset of cellularity for two-phase mixtures appears as an essential scientific issue. However, the mechanisms responsible for the development of cells structure for heterogeneous mixtures are not well understood. Experimental investigations are scarce and only a few theoretical studies can be found (Greenberg et al., 1999, Greenberg, 2007). The present study proposes an experimental approach to isolate and evaluate various potential mechanisms for a better comprehension of this domain.

An original experimental setup was employed to conduct both gaseous and two-phase experimentations of spherical expanding flames. An aerosol, with mono-sized and uniformly distributed droplets, was used as a simplified system for performing fundamental studies of well-controlled spray combustion.

Methodology

Three main processes of two-phase combustion have been selected as hypothetic mechanisms of the onset of cellularity,

a) The heat release of the burning flame evaporates the surrounding droplets: the droplets so act as a thermal sink on the flame (proportional to the latent heat of vaporization of the liquid fuel);

b) Due to evaporation, a gradient of gaseous fuel concentration is created around each droplet: this gradient locally changes the burning velocity, the temperature and modifies the mass and thermal diffusion between the reactive zone and the fresh gases, expressed in term of Lewis number;

c) If the liquid fuel is not fully evaporated before the arrival of the flame front, liquid droplets can be present in the reactive zone and interact within.

The heat sink phenomenon, induced by the droplet evaporation process, has been theoretically predicted by Greenberg et al. (1999) and described as having a major role on the spray flame cellularization. The gradient of gaseous fuel concentration is widely mentioned and computed in several studies carried on the evaporation and combustion of isolated droplet (Crespo and Linan, 1975, Ulzama and Specht, 2007, Kitano et al., 2014) and is created for spray flame in the said preheat zone, *i.e.* the zone where the temperature is high enough to vaporize the droplets, ahead the front flame. Finally, the last point c) was considered by Bradley et al. (2014) and they demonstrated that, in case of a sufficiently large diameter, it is possible for droplets to be present in the reaction zone and further enhance existing gaseous instabilities through the creation of more flame wrinkling.

The difficulty relies on study these phenomena in an independent manner in order to extract the relevant mechanisms. The present work proposes to focus on points a) and b); to investigate the heat sink effect and the local enrichment of fuel with the subsequent local Lewis number variations around droplets. Then the adopted strategy consists of amplifying the heat sink phenomenon and to suppress the gradient of gaseous fuel concentration aiming to obtain a controlled and constant Lewis number of the gaseous phase. To achieve this purpose, liquid fuel aerosol was replaced by an inert aerosol and water was selected because of its very high latent heat of vaporization and its well-established thermodynamic data under standard conditions. Additionally, two different gaseous flammable environments were selected to vary the Lewis number of the gaseous phase and so investigate the influence of non-equidiffusion and near-equidiffusion: namely a C_3H_8/air mixture and a CH_4/air mixture.

It is to be notified that the last point c) was discarded by using droplets sufficient small in order to have complete evaporation. Moreover, the local change in burning rate around the fuel droplets is not isolated here since the water droplet evaporation induces different local concentrations, which modifies the local burning rate.

2. Experimental device and procedure

The dual chamber

The experiments were conducted in a pressure-release type dual chamber which consists of a spherical combustion chamber (126 mm internal diameter) affording a volume of 1 L, centered in a high-pressure chamber of 11 L. The combustion chamber was filled with the flammable mixture while the high-pressure chamber was filled simultaneously with an inert gas (nitrogen) at the same pressure. The combustion chamber is equipped with 8 evacuation valves that open during combustion and the pressurized gases are evacuated from the combustion chamber toward the high-pressure chamber. As the high-pressure chamber is 10 times greater in volume than the combustion one, the pressure rise inside the internal combustion chamber is radically reduced for any initial pressure. The reader can refer to (Thimothée et al., 2015) for more details about the present dual chamber. This apparatus design allows safe operation and constant-pressure measurements which are well suited for flame instability studies, especially at high pressure (Tse et al., 2004). A representative schematic of the whole device is given on Fig. 1.

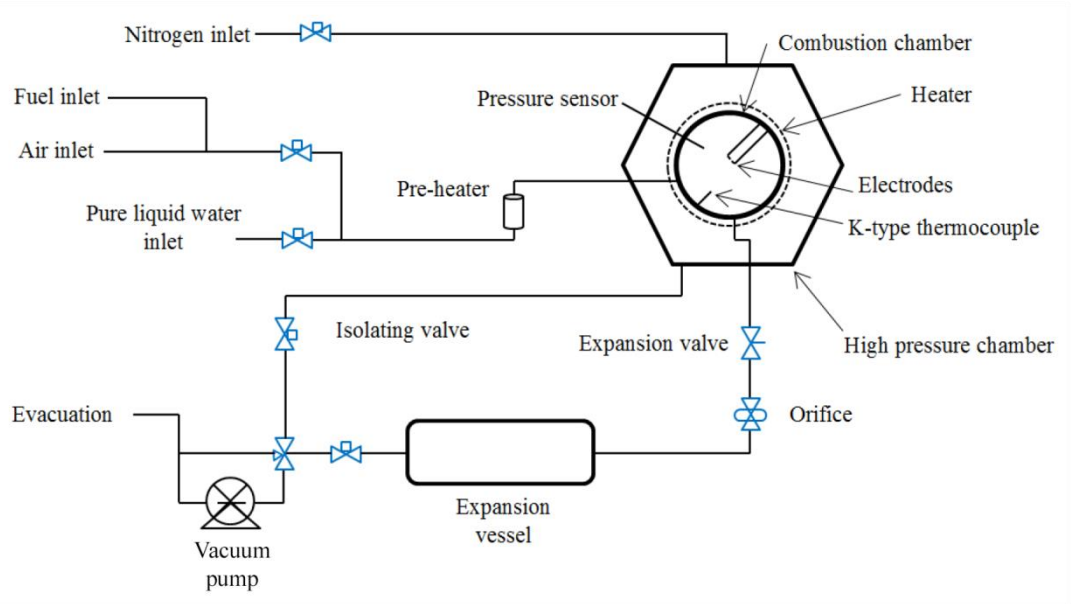

Figure 1. Schematic representation of the experimental apparatus.

Preparation of the gaseous mixture

After creating a vacuum, dry air and gaseous fuel are injected toward the combustion chamber through the use of mass flow meters. At the same time, a switching valve ensures the injection of an accurate and controlled volume of pure liquid water. The water is then mixed with the gaseous mixture air-fuel and is subsequently vaporized by a preheater before its arrival in the combustion chamber. An electric heating cable, rolled up around the combustion chamber, allows heating the fresh gases, thus maintaining the water in the gaseous state. The targeted equivalence ratio of the air-fuel environment is achieved by controlling the mass flow meters. The initial thermodynamic conditions of the quiescent gaseous mixture are the pressure P_1 and the temperature T_1.

The quantity of water vapor, present with the flammable mixture, can be defined as a dilution rate f, such that

$$f = \frac{n_w}{n_{tot}} \times 100 \quad with \quad n_w = \frac{\rho_w \cdot V_w}{M_w} \quad and \quad n_{tot} = \frac{P_1 \cdot V_{chamber}}{R \cdot T_1} \tag{1}$$

where n_w and n_{tot} are respectively the numbers of moles of water vapor and the number of moles of total gaseous mixture prepared in the chamber, V_w is the volume of injected liquid water, ρ_w and M_w are respectively the density and the molar mass of liquid water taken to be constant at $997\ kg/m^3$ and $0.018\ kg/mol$, $V_{chamber}$ the volume of the combustion chamber and R is the ideal gas constant.

Creation of the aerosol

Secondly, the droplet aerosol is generated from the initial gaseous mixture using the condensation technique of expansion cooling (based on the Wilson cloud chamber principle (Wilson, 1951)). This technique is widely recognized to create well-defined mono-size droplets uniformly distributed. To perform this, the combustion chamber is connected through a pipe to a 0.5 L expansion vessel. An expansion valve automatically controlled, with an adjustable orifice in order to enable the time of the pressure drop to be varied, is placed on the pipe to isolate the tank initially set to vacuum (see Fig. 1). The opening of the expansion valve induces a fast pressure drop that decreases the temperature of the gases in the combustion chamber. When the partial pressure of water exceeds its saturation pressure, the mixture undergoes a phase change which causes water droplets formation. The closing of the expansion valve ends the pressure drop and the heterogeneous mixture is centrally ignited by two tungsten electrodes. The thermodynamic two-phase conditions are the pressure P_2 and the temperature T_2 with the pressure and temperature drop parameters expressed as: $\Delta P = P_2 - P_1$ and $\Delta T = T_2 - T_1$.

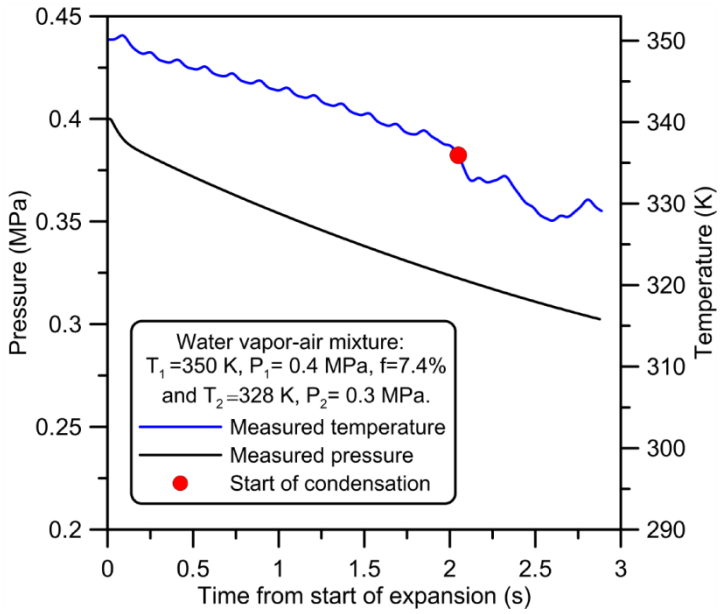

Figure 2. Typical temporal changes in pressure and temperature in the combustion chamber.

A K-type thermocouple of 13 μm in diameter and a pressure sensor are placed near-wall in the combustion chamber in order to control the temperature and the pressure during the filling process of the gaseous mixture and measure their variations during the expansion for the aerosol formation. The aerosol characterization (by laser diffraction particle size analyzer) and the pressure/temperature measurements were performed during preliminary calibration experiments without combustion and no fuel. It was checked that the methane and the propane have a negligible impact on the condensation process and thus also on the droplet formation. Fig. 2

shows typical temporal changes in pressure and temperature in the combustion chamber with an example of a mixture with $f = 7.4$ % expanded from $P_1 = 0.4\ MPa, T_1 = 350\ K$ to $P_2 = 0.3\ MPa, T_2 = 328\ K$.

Thermodynamic considerations

During the expansion process, only part of the water vapor condenses to form liquid droplets. Hence, when the combustion occurs, the mixture is composed of water both in liquid and vapor phases. The numbers of moles of liquid and water vapor are quantified using thermodynamic considerations together with temperature and pressure measurements. The number of moles of water vapor at the end of expansion $n_{vw(2)}$ is equal to:

$$n_{vw(2)} = \frac{P_{sat.}(T_2) \cdot V_{chamber}}{R \cdot T_2} \tag{2}$$

with $P_{sat.}(T_2)$ the saturation pressure at the temperature after expansion estimated using the Clausius-Clapeyron relation (Poling et al., 2001). Then the number of moles of liquid water condensed $n_{lw(2)}$ is deduced from the following equations:

$$n_{lw(2)} = n_{l(2)+vw(2)} - n_{vw(2)} \quad with \quad n_{l(2)+vw(2)} = \frac{f}{100} \times n_{tot(2)} \tag{3}$$

Once the expansion valve is opened, part of the total amount of mixture is evacuated and lost in the expansion tank. During this step the dilution rate of water f can be properly assumed to be constant. However, the overall number of moles (liquid + vapor) in the combustion chamber at the end of expansion must be re-evaluated (see Eq. (4)).

$$n_{tot(2)} = \frac{P_2 \times V_{chamber}}{R \cdot T_2} \tag{4}$$

Optical diagnostics

Two pairs of aligned transparent windows on the two chambers allow for optical access. A conventional shadowgraph system is employed in order to track the flame front displacement and to visualize the flame morphology. An Energetiq Laser-Driven-Light-Source is used as the light source and a high-speed camera (Phantom v1210) continuously records the flame evolution at 10,000 fps. The droplet diameter measurements of the aerosol were performed by means of a laser diffraction particle size analyzer (Sympatec HELOS).

3. Aerosol characterization

Statistical calculations are done from the droplet diameter data collected at each measurement and the Sauter Mean Diameter (SMD) is successfully used as a representative diameter of the aerosol. The number density N_d, defined as the number of droplets per unit of volume, was estimated from calculations based on the Beer-Lambert law evaluated at the wavelength $632.8\ nm$ of the laser particle size analyzer using droplet diameter values and laser attenuation measurements such that,

$$Tr = \frac{I}{I_0} = \exp[-\sigma_e \cdot N_d \cdot L] \quad with \quad \sigma_e = \frac{\pi}{4} \cdot \overline{Q_{ext.}} \cdot D_{20}^2 \tag{5}$$

where Tr is the measured laser transmittance, with I and I_0 the intensities of the attenuated and reference laser beam respectively, L the optical path length and σ_e the extinction cross-section defined by (Bachalo et al., 1988). The optical path length was measured from a window to another to $137\ mm$. The mean extinction efficiency

$\overline{Q_{ext.}}$ was taken to be 2.21 for water (Bohren and Huffman, 2008) and the surface mean diameter D_{20}, which is not directly measured by the particle size analyzer, can be reasonably approximated in case of a mono-size droplet aerosol by the arithmetic mean diameter D_{10}.

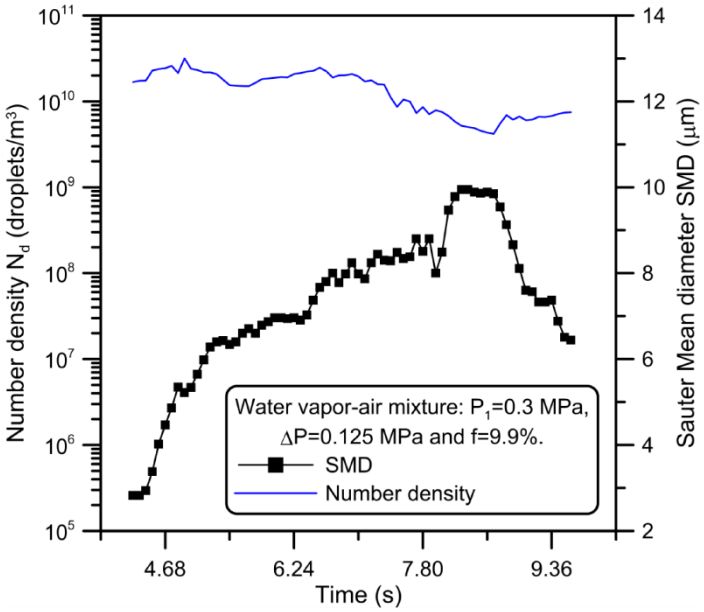

Figure 3. Typical evolution in SMD and number density with time of a water vapor-air aerosol during expansion.

Fig. 3 shows a typical temporal evolution in SMD and number density of a water-air mixture expanded from 0.3 to 0.175 MPa. The droplet diameter rapidly rises owing to nucleation and condensation until it reaches a maximum value. Then the droplets sizes tend to reduce due to heat transfer from the combustion chamber walls. The number density exhibits a near constant evolution during the expansion process. Droplet size data for the calculation of number density and for the selection of conditions for combustion experiments were considered only for the period between the start of droplet growth and peak value.

4. Flame speed determination

The temporal evolution of the flame radius noted $R_f(t)$ is extracted directly from the shadowgraph images using a post-processing program which fits the flame front, highlighted with the shadowgraph diagnostic, by a circle. The temporal evolution of the flame radius yields the flame propagation speed $V_S(t)$ with the following equation,

$$V_S(t) = \frac{dR_f(t)}{dt} \tag{6}$$

Then the stretch rate of the flame, noted κ, is evaluated with the following equation, where A, an element of flame surface, is equal to $A = 4 \cdot \pi \cdot R_f(t)^2$ in case of a spherical flame,

$$\kappa = \frac{1}{A} \cdot \frac{dA}{dt} = \frac{2}{R_f(t)} \cdot \frac{dR_f(t)}{dt} = \frac{2}{R_f(t)} \cdot V_S(t) \tag{7}$$

The unstretched (*i.e.* free of stretch) flame propagation speed, noted V_S^0, is after calculated by extrapolation to zero stretched of the values of V_S plotted in function of κ using the non-linear model (Kelley and Law, 2009, Halter et al., 2010) presented below,

$$\left(\frac{V_S}{V_S^0}\right)^2 \cdot ln\left(\frac{V_S}{V_S^0}\right)^2 = -\frac{2 \cdot L_b \cdot \kappa}{V_S^0} \quad (8)$$

where L_b is the Markstein length of burned gases. The reader is referred to (Thimothée et al., 2015) for more details about the method of flame speed determination with the present device. Fig. 4a shows examples of determination of unstretched flame propagation speeds for a rich propane-air mixture at 293 K for various initial pressures.

For constant pressure flame propagation, the fundamental laminar burning velocity S_L^0 is deduced from the unstretched flame propagation speed using the mass balance between fresh and burnt gases given by,

$$S_L^0 = \frac{\rho_b}{\rho_u} \times V_S^0 = \sigma \times V_S^0 \quad (9)$$

with σ the expansion factor defined as the ratio between the density of burned gases and that of fresh gases. These two values were computed using the EQUIL code where the GRI-mech 3.0 (Smith et al., 1999) was used for methane oxidation and the Wang-mechanism (Davis et al., 1999) for propane oxidation. Fig. 4b shows laminar burning velocity values obtained with the present experimental setup compared with recent experimental data from literature and data computed with PREMIX. Methane-air flames at $\phi = 0.9$ and propane-air flames at $\phi = 0.7$ were considered at 293 K in function of pressure. The values presented are the average value of three experiments and the standard deviation do not exceed 1 *cm/s*. Results show that laminar burning velocities are in good agreement with both numerical and experimental dataset, that validate the present apparatus for combustion studies in pressure.

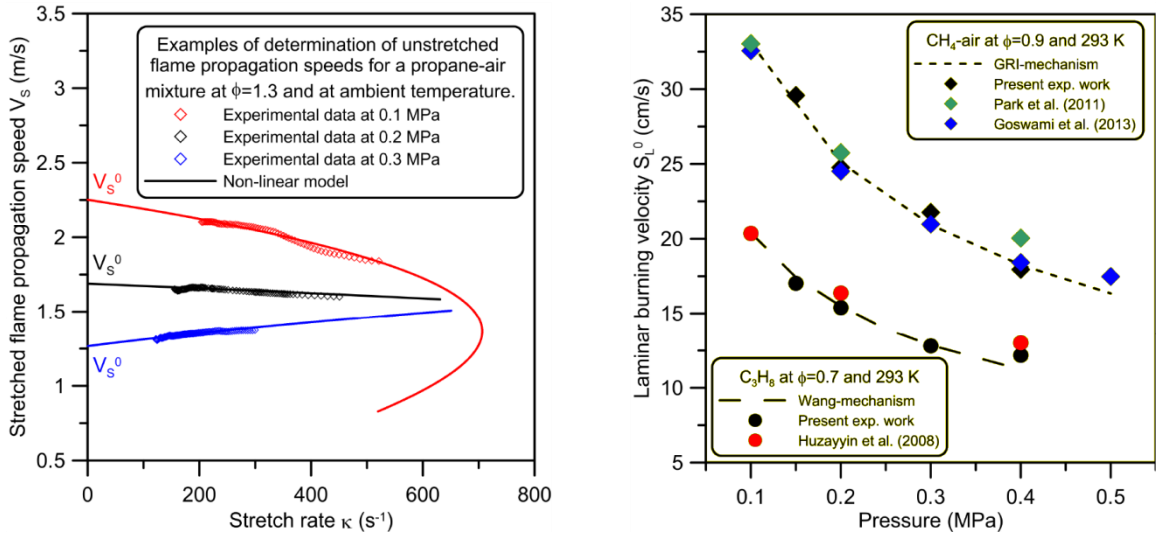

Figure 4. (a) Examples of determination of unstretched flame propagation speeds for a propane-air mixture at ϕ = 1.3 and 293 K for various initial pressures. (b) Laminar burning velocity values experimentally obtained for methane-air at ϕ = 0:9 and propane-air at ϕ = 0:7 in function of pressure at 293 K compared with experimental data from literature and numerical data from PREMIX.

5. Results

Experimental specifications

It exist two modes of instabilities: hydrodynamic and diffusional–thermal, which cause the onset of cellularities on the flame surface starting from a certain flame radius. Hydrodynamic instability is due to the density jump across the flame front which therefore is present for all flames. However diffusional–thermal instability is a result of the thermal and molecular diffusional properties of the fresh gases and may not be present for all flames. Diffusional-thermal mode occurs for non-equidiffusive flames which can either stabilize or destabilize the flame while is absent for equidiffusive flames. A proper way to quantify the intensity of this diffusive balance is to determine the global Lewis number. This non-dimensional number is defined as the ratio of the thermal diffusivity of the fresh gases over the molecular diffusivity of the limiting reactant in the abundant inert with $Le < 1$, $= 1$ and > 1, respectively, indicating unstable, neutral and stable cases. The definition from Addabbo et al. (2002) with the effective Lewis number $Le_{eff.}$ was also adopted as follows,

$$Le_{eff.} = 1 + \frac{(Le_E - 1) + (Le_D - 1) \cdot A}{1 + A} \quad with \quad A = 1 + Ze \cdot (\Phi - 1) \tag{10}$$

where Le_E and Le_D are respectively the Lewis number of the reactant that is in excess and deficient, Ze the Zeldovich number corresponding to $Ze = E_a \cdot (T_{ad.} - T_u)/R \cdot T_{ad.}^2$ with E_a the activation energy, $T_{ad.}$ the adiabatic flame temperature computed with the EQUIL code and T_u the temperature of the fresh gases. Here, Φ is defined as the ratio of the mass of excess-to-deficient reactants in the fresh mixture relative to their stoichiometric ratio (equal to ϕ for fuel-rich mixtures and $1/\phi$ for lean-fuel mixtures).

The activation energy E_a can be determined following the equation below (Egolfopoulos and Law, 1990),

$$\frac{E_a}{R} = \left(\frac{-2 \times \partial[\ln(\rho_u \cdot S_L^0)]}{\partial(T_{ad.}^{-1})} \right)_{\phi,P,T} \tag{11}$$

where the differential can be evaluated by calculating the quantities $\rho_u \cdot S_L^0$ and $1/T_{ad.}$for the given initial conditions of ϕ, P, and T by slightly varying its value through the substitution of a small quantity of nitrogen by argon. Computations were performed using the PREMIX code with typical percentages of substitution of nitrogen by argon from 0 to 9 %. The effective Lewis number definition allows a more rigorous estimation, especially for the stoichiometric value.

Figs. 5a and 5b show the calculation of both the effective Lewis number $Le_{eff.}$ and the global Lewis number Le for the two mixtures C_3H_8/air and CH_4/air against the equivalence ratio at atmospheric pressure and 350 K. For the methane-air mixture, the Lewis number is near to unity for all equivalence ratios with values slightly lower for lean cases and slightly higher for rich cases. The predominant thermal diffusivity for lean propane-air mixtures ($Le > 1$) tends to stabilize the flame whereas for the rich cases, the Lewis number is slightly lower than unity which tends the propane-air flames to be prone to cellularities induced both by hydrodynamic instabilities and thermo-diffusive instabilities.

Initial conditions for the water droplets experiments

Diameter and density number of water droplets were varied by changing the pressure drop ΔP (the size of the orifice was kept constant), the initial pressure P_1 and the water dilution rate f. In the present study, the

initial temperature was fixed to 350 *K*, the initial quantity of water was varied from 3 % to 10 %, two initial pressures of 0.3 *MPa* and 0.4 *MPa* were explored and several pressure drops were performed. A droplet diameter range of 6-11 μm and number densities between 0.5 and 2.10^{10} $droplets/m^3$ were covered. Small droplets were selected to ensure their complete evaporation before the arrival of the flame front and also to prevent any disruptive settling effect.

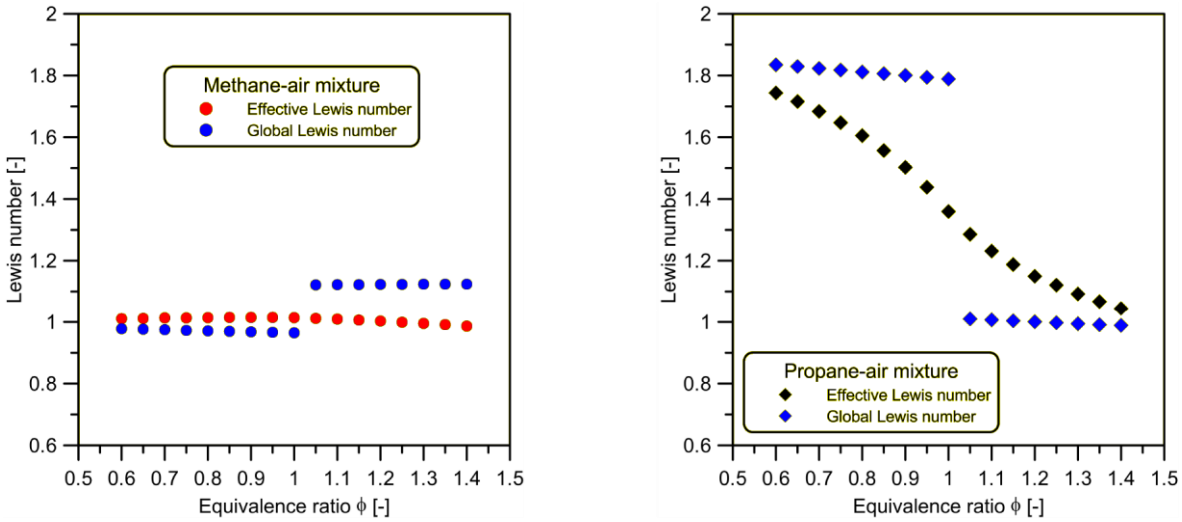

Figure 5. Calculation of the Lewis number against the equivalence ratio using the effective and the global definition for (a) methane (CH_4) in air and (b) propane (C_3H_8) in air at atmospheric pressure and 350 K.

Two equivalence ratios of 0.8 and 1.3 were selected for the propane-air mixture in order to investigate two sides of the diffusive balance ($Le > 1$ and $Le < 1$) and a stoichiometric equivalence ratio was considered for the methane-air mixture to investigate stable flames with a laminar burning velocities higher than for the propane-air flames.

Gaseous reference cases

Tests were performed to check the stability of the three different flammable environments selected. Experiments were realized at ambient temperature and for four initial pressures with no expansion process. The results are presented in Fig. 6 where the morphologies of the flames are shown at the same flame radius of about 22 *mm* (maximum radius accessible with the windows).

All the methane/air and lean propane/air flames are stable over the initial pressure range considered. The bright cracks appearing on the flame surface are due to the presence of electrodes. However rich propane-air flames become unstable after 0.3 *MPa* with few cells formation and are fully unstable at 0.4 *MPa* with a pebbled surface. For the lean propane-air mixture, the thermal-diffusional mode characterized by a high Lewis number stabilizes the flames. However, for the stoichiometric methane-air mixture and the rich propane-air one, the Lewis number is near unity. This means that these flames are not stabilized thermo-diffusively but only the rich propane-air case was observed cellular. The explanation can be found with the laminar burning velocity which is higher for the stoichiometric methane-air mixture than for the propane-air mixture at $\phi = 1.3$ whatever the pressure. The propane-air flame is more thermo-diffusively unstable than the methane at stoichiometry. The flames with the higher flame speeds will be more stabilized by stretch, so the methane-air flames are more stable.

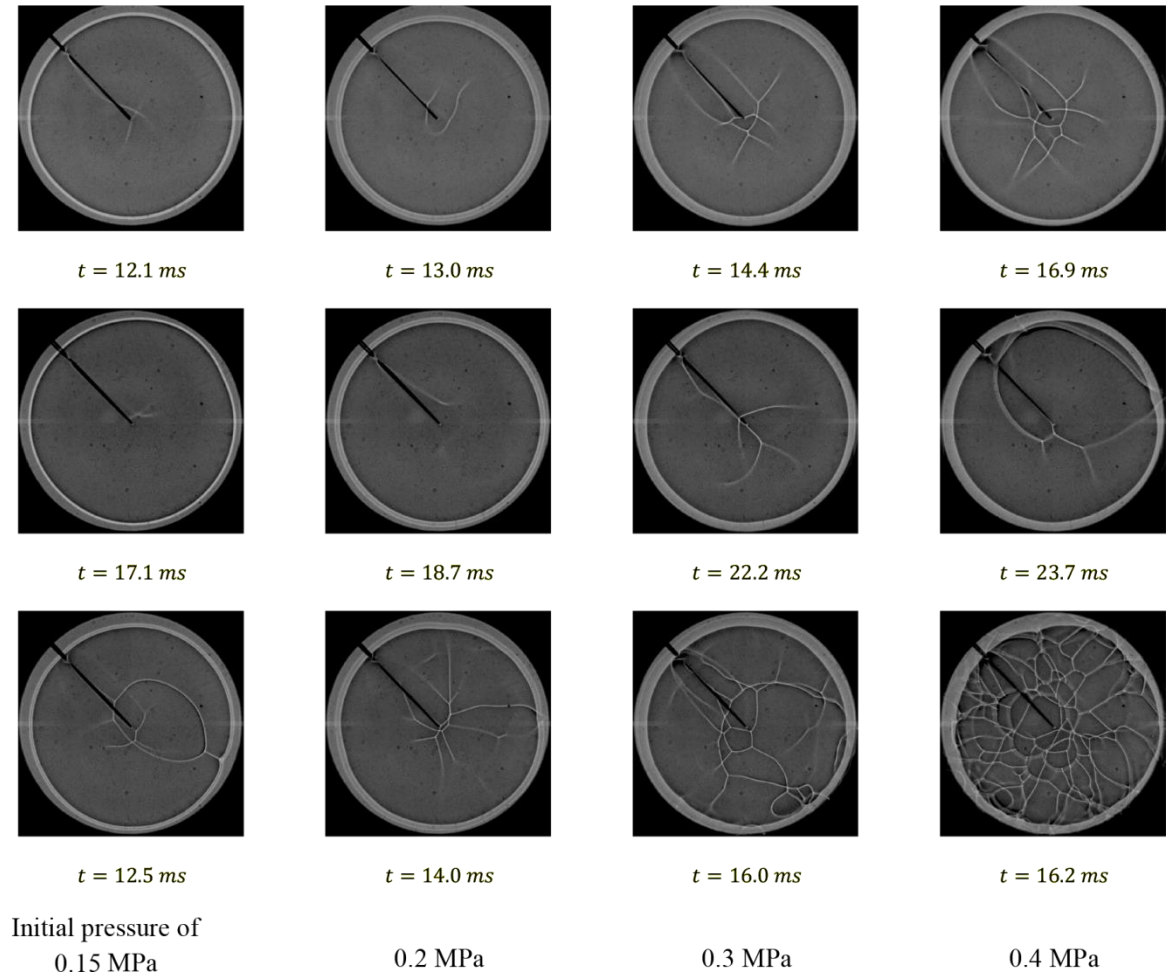

Figure 6. Stability of the three gaseous flammable mixtures with pressure evaluated at ambient temperature. First row: methane-air flames at ϕ = 1:0; second row: lean propane-air flames at ϕ = 0:8; and third row: rich propane-air flames at ϕ = 1:3.

Additionally, to obtain critical radii for the theoretical onset of instabilities, experimental observations were compared to critical Péclet numbers calculated from (Addabbo et al. (2002), Jomaas et al. (2007)). Experimental observations were found in accordance with expectations. For example, the critical radius for propane-air flame at $\phi = 0.8$ and 0.4 MPa was computed to $R_{cr.} = 84\ mm$ and for propane-air flame at $\phi = 1.3$ and 0.3 MPa, the critical radius was found to be $R_{cr.} = 20.5\ mm$. Lean propane-air flames are stable in the flame radius range explored and instabilities of rich propane-air flames are observable from 0.3 MPa, as it can be seen on Fig 6.

Study of the influence of water vapor

Only part of the water vapor is condensed and the remaining water vapor dilutes the air-fuel mixture. Thus, it is important to ensure that the water vapor resulting from the aerosol formation does not modify the thermal-diffusional property controlled by the two air-fuel mixtures. The Lewis number was therefore computed using the global definition for the three cases against a realistic water dilution rate range (below the lower flammability limit) (Saito and Liao, 2005). Fig. 7 demonstrates that the Lewis number changes very slightly with the water dilution rate. The thermal-diffusional properties of the gaseous environments are not modified by the presence of water vapor. Moreover, the chemical effect of the water vapor is considerably lower than the thermal effect and has been assumed to be negligible (Lentati and Chelliah, 1998).

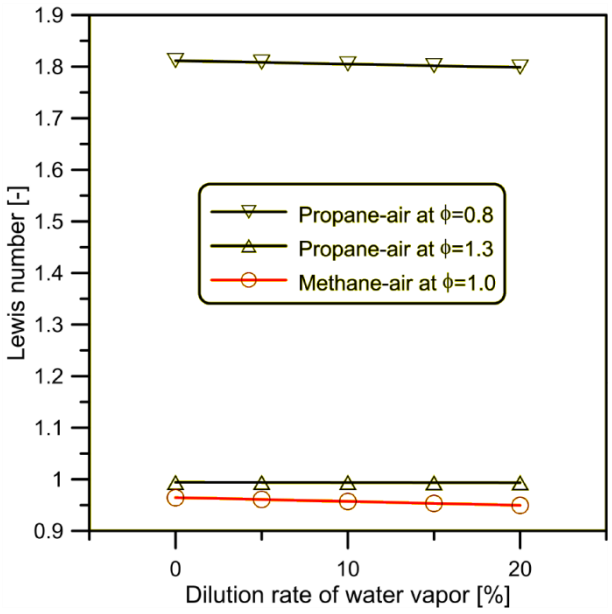

Figure 7. Lewis number for a propane-air mixture at ϕ = 0:8 and ϕ = 1:3 and for a stoichiometric methane-air mixture against the dilution rate of water vapor.

Additional experiments were performed with water vapor to validate its negligible effect on the flame stability. Gaseous combustions with water vapor addition were realized at 350 *K* with the rich and the lean propane-air mixtures for the same initial pressures of 0.15, 0.2, 0.3 and 0.4 *MPa* and by varying the water vapor content between 0 and 10 % in accordance with the conditions of the water aerosol experiments. Flame structures were considered at the same flame radius of 22 *mm* and the morphologies were found very similar compared to gaseous reference flames (without water vapor), which support the Lewis number calculations (Fig. 7).

The addition of water vapor is known to inhibit the reactivity of a flammable mixture which results in a decrease of the burning velocity whatever the equivalence ratio (Vancoillie et al., 2013, Mazas et al., 2011). The effect of the water vapor content on the laminar burning velocity is presented in Fig. 8. Only a lean propane-air mixture is shown. Experimental results for *T=350 K* and two pressure conditions are compared to computations done using the Wang-mechanism. The values presented are the average value of three experiments and the standard deviation do not exceed 1 *cm/s*. The laminar burning velocity decreases with the water dilution rate in a quasi-linear trend for all the pressure conditions, which is well reproduced by the model. The laminar burning velocity reduction was found similar for the rich propane-air mixture.

It is to be notified that gaseous flames with a low flame speed displacement (around 15 *cm/s*) are very slightly deformed and maintain an overall spherical shape. Therefore, such velocity reductions, due to the presence of water vapor in the gaseous phase, were found negligible on the onset of cellularities.

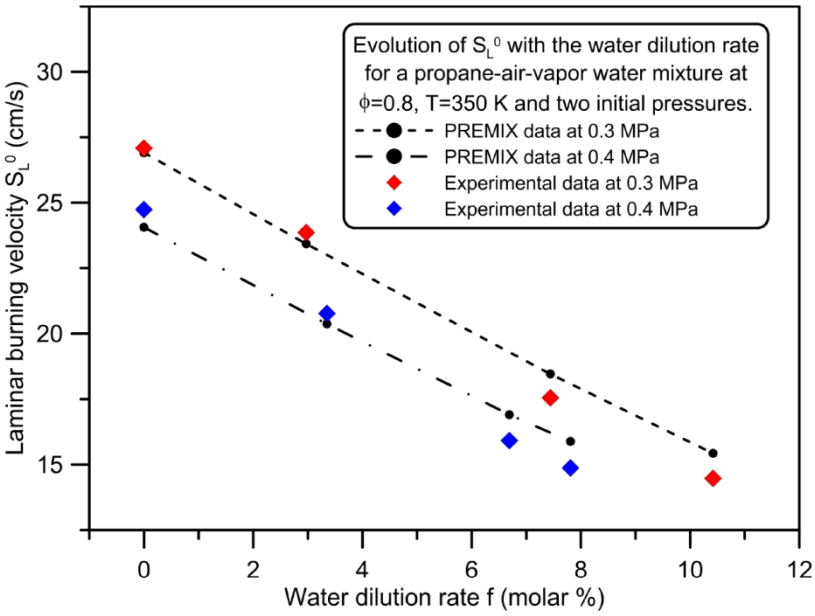

Figure 8. Influence of the water vapor on the laminar burning velocity for a lean propane-air mixture at 350 K.

Water aerosol flames

As illustrated in Fig. 9, three different regimes of propagation may be identified: 1) stable and smooth flame propagation; 2) cellular flame propagation and 3) no propagation (characterized by vanished flame). Based on these observations, diagrams were built for the three different air-fuel environments with the initial quantity of water f and the pressure after expansion P_2 (at the moment of ignition for the aerosol combustion). Results are presented in Fig. 10.

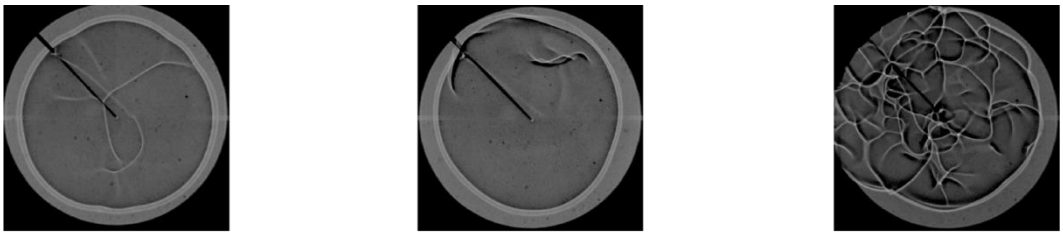

$P_2 = 0.2\ MPa$ $P_2 = 0.3\ MPa$ $P_2 = 0.3\ MPa$

Figure 9. Examples of shadowgraph frames. Left: methane-air-water flame aerosol at stoichiometry. Middle: propane-air-water flame aerosol at ϕ = 0:8. Right: propane-air-water flame aerosol at ϕ = 1:3.

Firstly, the "no propagation" cases were encountered for methane-air-water and lean propane-air-water flames due to the high latent heat of vaporization of liquid water. Rich propane-air-water flames have always propagated. A possible explanation is that for this fuel and at this equivalence ratio, the heat released by the flame is higher compared to the two other cases.

Cellular flames were observed only for some rich propane-air-water flames. Cellularities only appear for the near-equidiffusive mixture (Lewis number slightly lower than unity) for which the homogeneous gaseous flame is unstable. In other words, the presence of a heterogeneous phase without local Lewis number variations does not trigger cellular instabilities.

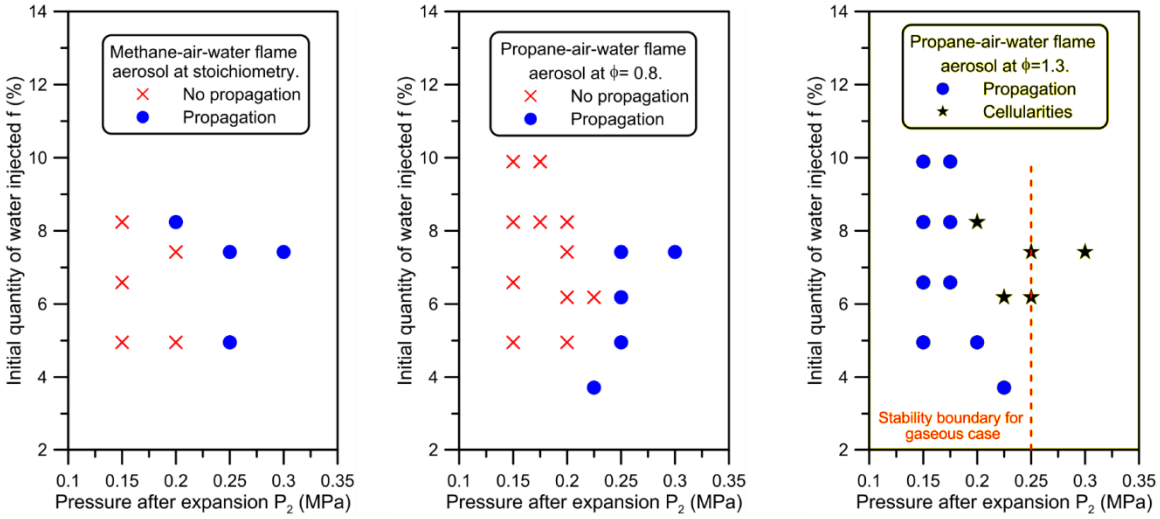

Figure 10. Diagram of flame observations with the initial conditions for the three water aerosol-air-fuel mixtures.

Nevertheless, it can be seen that the instabilities observed with water aerosols appear at slightly lower pressures (about 0.2 *MPa*) than for gaseous cases (0.3 *MPa*). This result is discussed in the following part.

Heat sink phenomenon

To go further, calculations of overall energies were done in order to highlight the heat sink phenomenon. For this, the heat of vaporization (Q_v), needed to evaporate the droplets, and the heat released by the flame (Q_f) were quantified with the two equations below,

$$Q_v = L_v \cdot n_{lw(2)} \cdot M_{water} \quad and \quad Q_f = LCV \cdot X_{fuel} \times n_{tot(2)} \tag{12}$$

with L_v the heat of vaporization of water taken to be 2260 kJ/kg, X_{fuel} the molar fraction of the fuel and LCV the lower calorific value of the fuels respectively (803.3 kJ/mol for methane and 2044.1 kJ/mol for propane). Then, all flame observations are plotted in a single diagram (Fig. 11) for the three water-air-fuel mixtures with non-dimensional parameters: the ratio of the heat of vaporization over the heat released by the flame (to quantify the heat sink phenomenon) for abscissa and the ratio of the mean droplet interdistance a over the SMD to represent the water aerosols for the vertical axis. The mean droplet interdistance, noted a, was directly estimated from the number density such as: $a = \sqrt[3]{1/N_d}$ according to (Annamalai and Ryan, 1992).

Thanks to the high heat of vaporization of water, a clear boundary separates the “propagation” cases to the “no propagation” ones which are located in a region of high Q_v/Q_f values. Then it can be distinguished that the droplet size and the density number have an influence on the flame extinction phenomenon. However, no boundary appears for the “unstable propagation” cases which are scattered with the “stable propagation” ones meaning that the thermal sink effect is not a mechanism responsible for the trigger of cellular instabilities.

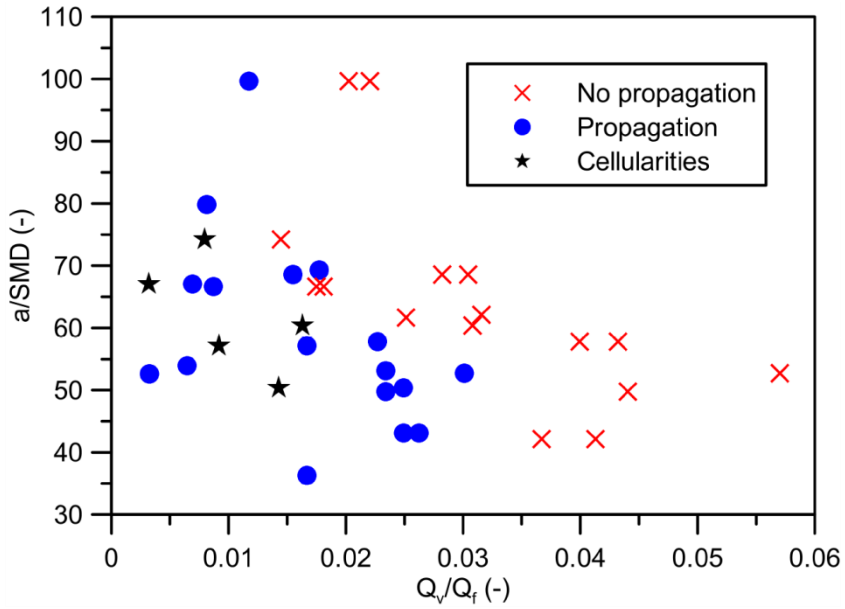

Figure 11. Diagram of flame observations highlighting the heat sink phenomenon due to water droplets. Experimental observations from stoichiometric methane-air flames, lean and rich propane-air flames for all pressures (0.15, 0.175, 0.2, 0.225, 0.25, and 0.3 MPa).

Comparison between single and two-phase flame speed

The flame speeds of "water aerosol" cases are compared in Table 1 with their gaseous counterpart with water vapor for the "cellular propagation" observations (third diagram of Fig. 10 with the rich propane-air-water flames). We endeavored to compare the values at the same conditions of pressure P_2, temperature T_2 and same overall quantity of water f. The molar percentage of liquid water which has condensed is reported, based on the calculations of the number of moles of liquid and gaseous water respectively present after expansion (see Eqs. (2), (3) and (4)). Owing to the heterogeneous aspect of water aerosols, the comparison was made using the unstretched flame propagation speed parameter (Lawes et al., 2006). Some flames are somewhat deformed but the small size of the water droplets prevents any settling effect, reducing the buoyancy impact on the flames. Motion of flames due to convection (relative to the center defined by the electrodes) is hardly noticeable.

Experimental initial conditions			Aerosol flames		Gaseous counterpart flames
f (%)	P_2 (MPa)	T_2 (K)	V_S^0 (m/s)	Molar % of liquid water condensed	V_S^0 (m/s)
6.2	0.25	317	0.61	36.9	1.03
7.4	0.25	317	0.30	47.1	0.93
7.4	0.3	328	0.49	10.6	0.88
8.2	0.2	323	0.73	23.4	1.02
6.2	0.225	309	0.31	58.6	1.08

Table 1. Comparison of the flame speed between the water droplets case and the counterpart homogeneous gaseous case for the "cellular propagation" observations of the rich propane-air-water mixtures.

The results show that all the speed values of the aerosol flames are greatly lower than the fully vaporized cases taken in the same overall conditions. All the cases considered are cellular but the thermal effect of the water

droplets is strong enough to systemically slow down the flame speed. The flame speed of the water droplets is so reduced that the flame stretch rate, for a given flame radius, is greatly lower than for the gaseous flames (burning velocity is proportional to the stretch rate for a given flame radius, see Eq. (7)). Such a decrease of the flame stretch rate thus allows explaining the premature apparition of cellular instabilities (observed on the third diagram of Fig. 10) in case of a water aerosol compared to the fully vaporized case due to a decrease of the radius of cells occurrence. So the thermal effect led to a high flame speed decrease which in turn favors a lower stretch rate and lets the cellular instabilities appear slightly earlier.

6. Summary and conclusion

- A dual chamber was successfully employed in order to study cellular instabilities of both gaseous and heterogeneous mixtures.
- An experimental strategy was developed with a water aerosol configuration, which has been demonstrated as a proper inert aerosol, in order to conduct a fundamental study on the mechanisms of cellular instabilities for a two-phase flame.
- Water mist was successfully employed together with two different thermal-diffusional gaseous environments in order to amplify the heat sink effect of the droplets and in order to eliminate the local Lewis number variations by imposing a constant and controlled value.
- Diagrams were built to exhibit flame observations with relevant parameters and used to highlight the thermal sink phenomenon.

The experiments showed that the cellular instabilities of the two-phase mixtures only appear in the case where the fully vaporized mixture is also unstable with a development of cells. In other words, a heterogeneous phase with no Lewis number variations does not change the onset of instabilities compared to the homogeneous gaseous phase. The onset of cellular instabilities for two-phase flames is ruled by the same mechanism that for gaseous mixtures where the Lewis number is a key parameter.

Regarding the thermal effect of the droplets, it has been found to considerably reduce the flame speed of the flame aerosols compared to the homogeneous gaseous cases. In addition, the thermal effect can cause extinction phenomena and can also, in certain cases, reduce the flame radius of cell occurrence. However, the thermal sink effect was demonstrated not to have a major role in the onset of cellular instabilities for two-phase flames.

Finally, the results suggest that the gradient of fuel concentration forming around the droplets is the most significant mechanism of cell development by affording locally a suitable diffusivity disparity with a Lewis number close or less than unity. This conclusion can, for example, explain the observations of cellular lean air-fuel aerosols while the counterpart gaseous mixture is totally smooth and stable (Thimothée et al., 2015). Moreover, it is reasonable to think that the other local variations induced by a local fuel enrichment around the droplet are ineffective.

7. Acknowledgements

This work was supported by a joint grant from the CNES and the Région Centre. The authors gratefully acknowledge the support of the CNES and the CNRS though the GDR MFA n°2799 for their financial support

8. References

Addabbo, R., Bechtold, J. & Matalon, M. (2002) Wrinkling of spherically expanding flames. *Proc. Combust. Inst.,* **29,** 1527.

Annamalai, K. & Ryan, W. (1992) Interactive processes in gasification and combustion. Part I: Liquid drop arrays and clouds. *Prog. Energ. Combust.,* **18,** 221.

Bachalo, W., Rudoff, K. & Brena De La Rosa, A. (1988) Mass flux measurments of a high number density spray system using the phase Doppler particle analyzer. *26th Aerospace Science Meeting: Reno, Nevada*.

Ballal, D. & Lefebvre, A. (1981) Flame propagation in heterogeneous mixtures of fuel droplets, fuel vapor and air. *Proc. Combust. Inst.,* **18**, 321.

Bohren, C. F. & Huffman, D. R. (2008) Absorption and scattering of light by small particles. John Wiley & Sons.

Bradley, D., Lawes, M., Liao, S. & Saat, A. (2014) Laminar mass burning and entrainment velocities and flame instabilities of i-octane, ethanol and hydrous ethanol/air aerosols. *Combust. Flame,* **161,** 1620.

Crespo, A. & Linan, A. (1975) Unsteady effects in droplet evaporation and combustion. *Combust. Sci. Technol.,* **11,** 9.

Davis, S., Law, C. & Wang, H. (1999) Propene pyrolysis and oxidation kinetics in a flow reactor and laminar flames. *Combust. Flame,* **119,** 375.

Egolfopoulos, F. & Law, C. (1990) Chain mechanisms in the overall reaction orders in laminar flame propagation. *Combust. Flame,* **80,** 7.

Goswami, M., Derks, S. C., Coumans, K., Slikker, W. J., de Andrade Oliveira, M. H., Bastiaans, R. J., Luijten, C. M., de Goey, L. P. H. & Konnov, A. A. (2013) The effect of elevated pressures on the laminar burning velocity of methane+ air mixtures. *Combust. Flame*, **160**, 1627.

Greenberg, J. B. (2007) Finite-rate evaporation and droplet drag effects in spherical flame front propagation through a liquid fuel mist. *Combust. Flame,* **148,** 187.

Greenberg, J. B., Mcintosh, A. & Brindley, J. (1999) Instability of a flame front propagating through a fuel-rich droplet-vapour-air cloud. *Combust. Theor. Model.,* **3,** 567.

Halter, F., Tahtouh, T. & Mounaïm-Rousselle, C. (2010) Measurement of laminar burning speeds and Markstein lengths using a novel methodology. *Combust. Flame,* **156,** 1735.

Hayashi, S., Kumagai, S. & Sakai, T. (1977) Propagation velocity and structure of flames in droplet-vapor-air mixtures. *Combust. Sci. Technol.,* **15,** 169.

Huzayyin, A. S., Moneib, H. A., Shehatta, M. S., & Attia, A. M. A. (2008) Laminar burning velocity and explosion index of LPG–air and propane–air mixtures. *Fuel,* **87**, 39.

Jomaas, G., Law, C. K. & Bechtold, J. K. (2007) On transition to cellularity in expanding spherical flames. *J. Fluid Mech.,* **583**, 1.

Kelley, A. & Law, C. (2009) Nonlinear effects in the extraction of laminar flame speeds from expanding spherical flames. *Combust. Flame,* **156,** 1844.

Kitano, T., Nishio, J., Kurose, R. & Komori, S. (2014) Effects of ambient pressure, gas temperature and combustion reaction on droplet evaporation. *Combust. Flame,* **161,** 551.

Lawes, M., Lee, Y. & Marquez, N. (2006) Comparison of iso-octane burning rates between single-phase and two-phase combustion for small droplets. *Combust. Flame,* **144,** 513.

Lentati, A. & Chelliah, H. (1998) Physical, thermal, and chemical effects of fine-water droplets in extinguishing counterflow diffusion flames. *Proc. Combust. Inst.,* **27**, 2839.

Lin, T. & Sheu, Y. (1991) Theory of laminar flame propagation in near-stoichiometric dilute sprays. *Combust. Flame,* **84,** 333.

Mazas, A., Fiorina, B., Lacoste, D. & Schuller, T. (2011) Effects of water vapor addition on the laminar burning velocity of oxygen-enriched methane flames. *Combust. Flame,* **158,** 2428.

Myers, G. & Lefebvre, A. H. (1986) Flame propagation in heterogeneous mixtures of fuel drops and air. *Combust. Flame,* **66,** 193.

Nomura, H., Izawa, K., Ujiie, Y., Sato, J. I., Marutani, Y., Kono, M. & Kawasaki, H. (1998) An experimental study on flame propagation in lean fuel droplet-vapor-air mixtures by using microgravity conditions. *Proc. Combust. Inst.,* **27**, 2667.

Park, O., Veloo, P. S., Liu, N., & Egolfopoulos, F. N. (2011) Combustion characteristics of alternative gaseous fuels. *Proc. Combust. Inst.,* **33**, 887.

Poling, B. E., Prausnitz, J. M. & O'connell, J. P. (2001) The properties of gases and liquids. McGraw-Hill New York.

Saito, N. & Liao, C. (2005) Suppression Effect of Water Vapor on Flammability Limits of Hydrocarbon Fuels--A Study on Fire Suppression by Water Mist. *6th Asia-Oceania Symposium on Fire Science and Technology: Daegu, Korea*.

Smith, G. P., Golden, D. M., Frenklach, M., Moriarty, N. W., Eiteneer, B., Goldenberg, M., Bowman, C. T., Hanson, R. K., Song, S. & Gardiner Jr, W. C. (1999) GRI-Mech 3.0.

Thimothée, R., Chauveau, C., Halter, F. & Gökalp, I. (2015) Characterization of Cellular Instabilities of a Flame Propagating in an Aerosol. *Proceedings of ASME Turbo Expo 2015: Turbine Technical Conference and Exposition: Montréal, Canada*.

Tse, S. D., Zhu, D. & Law, C. K. (2004) Optically accessible high-pressure combustion apparatus. *Rev. Sci. Instrum.,* **75,** 233.

Ulzama, S. & Specht, E. (2007) An analytical study of droplet combustion under microgravity: Quasi-steady transient approach. *Proc. Combust. Inst.,* **31,** 2301.

Vancoillie, J., Christensen, M., Nilsson, E., Verhelst, S. & Konnov, A. (2013) The effects of dilution with nitrogen and steam on the laminar burning velocity of methanol at room and elevated temperatures. *Fuel,* **105,** 732.

Wilson, J. G. (1951) The principles of cloud-chamber technique. Cambridge University Press.